Study on Optoelectronic, Thermoelectric and Mechanical Properties of Lead Free Oxide Double Perovskite Ca_2VTlO_6

Roll: 191311
Session: 2019–2020

Report submitted to the Department of Physics at
Jashore University of Science and Technology
in partial fulfillment of the requirements
for the degree of Bachelor of Science
with Honours in Physics

May 2025

Abstract

In this study, we employ first-principles calculations to systematically investigate the structural, mechanical, electrical, optical, and thermal properties of the oxide double perovskite compound Ca_2VTlO_6. The electronic band structure of the oxide double perovskite Ca2VTlO6 is examined by density functional theory (DFT) within the generalized gradient approximation (GGA) using the modified Becke–Johnson (mBJ) potential, implemented in the WIEN2k code. The compounds exhibit perfect cubic symmetry with the space group $Fm\bar{3}m$ (225). Mechanical properties confirm that Ca_2VTlO_6 is brittle. According to the electrical property investigation, Ca_2VTlO_6 has an indirect band gap of 2.327 eV. The density of states (DOS) is determined, providing insight into the energy band gap. The optical properties are investigated using the dielectric function, absorption coefficient, optical conductivity, reflectivity, and refractive index. These properties show a notable response in the ultraviolet and visible regions, making the materials well-suited for photocell and optoelectronic device applications. The thermoelectric properties of the compound are characterized using the BoltzTraP code, with a focus on electrical conductivity, thermal conductivity, power factor, Figure of merit, and Seebeck coefficient. At room temperature, the estimated value of the figure of merit is 0.79 for Ca_2VTlO_6. These values suggest that Ca_2VTlO_6 has the potential to be a material for thermoelectric device applications.

Acknowledgements

Firstly, I praise and thank Creator , the Lords of the worlds, the owner of life and death. Secondly, I would like to express my gratitude to my respected supervisor, Dr.Mohammad Abdur Rashid, for his continuous guidance and support that help me to complete my project work properly. During the period of this project, he always shows me invaluable confidence and at the same time, he has helped me as a mentor, advising me on what should be done and what should not be done. His counsel and self motivation have significantly bolstered my confidence to move forward.

I want to express my gratitude to the Quantum Materials Simulation Lab (QMSL) members who supported me throughout the project, both directly and indirectly. They instructed me in the precise calculation of all relevant characteristics and imparted extensive knowledge that enabled me to produce a comprehensive project report. Furthermore, QMSL offered several essential facilities, including computational facilities. Without this facilities, i cannot calculate my any property of the system. Because I didn't have my own computer or laptop. Other facilities also include printing services. I would never forget to thank my parents and elder sister from the bottom of my heart for their love, unconditional support, and prayers in all stages of my life. Their love and encouragement always give me mental support to continue my study smoothly.

Contents

Study on Optoelectronic, Thermoelectric and Mechanical Properties of Lead Free Oxide Double Perovskite Ca_2VTlO_6

List of Figures

List of Tables

Study on Optoelectronic, Thermoelectric and Mechanical Properties of Lead Free Oxide Double Perovskite Ca_2VTlO_6

Chapter 1

Introduction

With time, the growing energy demand and the alarming depletion of existing energy sources have driven the scientific community to investigate new renewable energy resources [1]. Over the past decade, double perovskite materials; have attracted much attention due to their promising application in different field, such as light-emitting diodes(LEDs), lasers, radiation detectors, and solar cells [2–5]. The use of these materials is revolutionizing almost every aspect of human life, including entertainment, transportation, communication, healthcare, and even personal interactions [6].

In recent years, these materials have gained significant attention as innovative solutions for optoelectronic and thermoelectric applications, driven by their outstanding energy-harvesting performance. Optoelectronic materials are specifically designed to convert light into electrical signals with high efficiency, whereas thermoelectric materials are engineered to transform waste heat into usable energy. Direct band gap semiconductors are preferred for optoelectronic devices, whereas narrow band gap materials are favored for thermoelectric applications [7,8]. Among various types of double perovskites, lead-based DP materials demonstrate exceptional potential in photovoltaic technologies due to their optimal direct band gap, high absorption properties, and favorable effective masses of charge carriers [9–12]. The use of lead had to be discontinued due to its toxicity and instability [13]. Double perovskites

demonstrate high efficiency in various applications, offering exceptional stability through the use of non-toxic, environmentally sustainable materials [14–16]. In recent years, researchers have explored double perovskites (DPs) by replacing Lead (Pb) with combinations of monovalent and trivalent cations. These compounds follow the formula $A_2BB'X_6$, where A signifies a large cation like Cs^+, B and B′ represent monovalent and trivalent cations, respectively and X stands for halides or oxygen [17]. The analysis of different combinations of the B and B′ cations is expected to provide opportunities to discover suitable high-efficiency Pb-free double perovskites. For the B site, possible candidates include K^+, Rb^+, Ag^+, In^+ and Au^+, while for the B′ site, potential choices include Sb^{3+}, Bi^{3+} and others [18]. The fundamental structure of oxide based double perovskites is $A_2BB'O_6$ [19].

In this structure, A represents an alkaline-earth or rare-earth ion. In perovskites, the B-sites, which are transition metal sites, are alternately occupied by distinct cations, B and B′. Each pair B and B′ is bridged by oxygen atoms, resulting in alternating BO_6 and $B'O_6$ octahedra. This type of compound generally forms ideal cubic structures belonging to space group no 225 ($Fm\bar{3}m$). These materials exhibit various magnetic properties, including ferromagnetism, antiferromagnetism, and ferrimagnetism, which depend on the specific metal ions involved. For instance, La_2NiMnO_6 and Sr_2FeMoO_6 display ferromagnetism and magnetoresistance, making them promising candidates for spintronics applications [20, 21]. Certain double perovskite compounds display superconducting properties at low temperatures. A notable example is double-perovskite Bismuth oxides, which have shown significant efficiency in superconductivity applications. Here are just a few examples of research conducted with double perovskite oxides. The field is extensive and ongoing research continues to explore their distinct properties and potential applications in diverse scientific and technological domains. The unstable structure, high humidity, and environmental pollution associated with lead-based DPs limit their practical applications. Consequently, the search for stable, eco-friendly, and non-toxic DP materials has obtained significant attention in recent year.

In our study, we investigated the structural, electronic, optical, mechanical, and

thermal properties of Ca_2VTlO_6 double perovskites using a first-principles approach. Using DFT calculations, we aim to explore the atomic and electronic structures of Ca_2VTlO_6, assess its stability, and investigate its electronic band structure. The high structural and thermodynamic stability emphasizes their potential for both solar cell and thermoelectric applications. Until now, there have been only a limited number of experimental and theoretical studies on these materials. Therefore, for energy systems, we believe this study provides a solid foundation and proper guidance for utilizing these compositions.

This project is divided into four Chapter, starting with the introduction. In Chapter 2 the Schrödinger equation for charge particle is discussed and extended to generalized many body Schrödinger equation for a system consisting of electrons and nuclui, neglecting external magnetic and electric fields. This chapter also discusses an advance theoretical approach, Density Functional Theory which systematically transforms the many body problem without explicit electron-electron interactions. Hartree- Fock method, a traditional approach is discussed for finding appropriate solution to the wave function and energy of a quantum many-body system in stationary state. At the end of this Chapter various approximation are discussed for determining the exact functionals for exchange and correlation. In chapter 3, the structural,electronic, optical, mechanical and thermal properties are discussed in details. Finally, the Chapter 4 contains summary of this work.

Chapter 2

Theory

2.1 Basic Quantum Mechanics

To understand the foundation of Density Functional Theory(DFT), it is essential to first review the fundamental principles of quantum mechanics. Quantum mechanics provides the framework for describing the behavior of particles at the atomic and subatomic levels. Central to this framework is the Schrödinger equation, which governs the dynamics of quantum systems and allows us to derive important properties such as energy levels and wave functions. The Schrödinger equation can be expressed in both time-dependent and time-independent forms. We will focus on the time-independent Schrödinger equation, which is particularly relevant for stationary states of quantum systems. The solutions to this equation give wave functions that describe the likelihood of where particles are located and how they move, as well as energy eigenvalues that represent possible energy levels of the system. Together, these help us to understand how electrons behave in atoms and molecules.

2.1.1 Schrödinger Equation

The Schrödinger equation, formulated by Erwin Schrödinger in 1925, is a key equation in quantum mechanics that describes the quantum state of a physical system,

essential for understanding the behavior of particles like electrons, photons, and other quantum objects.

$$\hat{H}\Psi(\mathbf{r}) = E\Psi(\mathbf{r}) \tag{2.1}$$

Where, $\hat{H}$ is the Hamiltonian operator, Ψ is the wave function of the system, and E is the energy eigenvalue to the quantum state described by Ψ. This equation is crucial in finding the stationary states of quantum systems. The Hamiltonian, $\hat{H}$, represents the total energy operator of the system and is typically composed of two parts: The kinetic energy operator, $\hat{T}{=}-\frac{\hbar^2}{2m}\nabla^2$ and the potential energy operator, $\hat{V}{=}V(\mathbf{r})$. The kinetic energy operator describes the motion of particles, while the potential energy operator accounts for the forces acting on them due to their positions within the system. Together, these components determine the total energy of the quantum system . Hence, The Schrödinger equation for three dimensions becomes

$$-\frac{\hbar^2}{2m}\nabla^2\Psi(\mathbf{r}) + V(\mathbf{r})\Psi(\mathbf{r}) = E\Psi(\mathbf{r}). \tag{2.2}$$

2.1.2 Wave Function and Probability Density

The wave function, Ψ, is a fundamental concept in quantum mechanics that encodes all information about a system's quantum state, including the probability of finding particles at specific positions and with particular properties. While Ψ itself lacks direct physical meaning, its square, $|\Psi(\mathbf{r})|^2$ represents the probability distribution of particle positions, essential for calculating observable properties and understanding particle behavior [22, 23].

2.2 The Many–Body Problem

The many–body problem in quantum mechanics addresses the challenge of describing systems comprising multiple interacting atoms. Unlike single-atom systems, which can often be analyzed using analytical solutions, many–body systems involve intricate interactions that lead to emergent phenomena, such as correlation and collective behaviors [24]. The Hamiltonian of many–body system consisting of nuclei

and electrons can be written as,

$$\hat{H} = \hat{T}_{nuclui} + \hat{T}_{electrons} + \hat{V}_{nn} + \hat{V}_{ee} + \hat{V}_{ne} \tag{2.3}$$

With the term representing:

- $\hat{T}_{nuclei}$:the kinetic energy for the nuclei,
- $\hat{T}_{electrons}$:the kinetic energy for the electrons,
- $\hat{V}_{nn}$:the nucleus-nucleus Coulomb repulsion,
- $\hat{V}_{ee}$:the electron -electron Coulomb repulsion,
- $\hat{V}_{ne}$:the attractive interaction between nuclei and electrons.

These interaction terms make solving the Schrödinger equation for large systems of atoms exceedingly complex. The Coulomb interactions $\hat{V}_{nn}$, $\hat{V}_{ee}$, $\hat{V}_{ne}$ describe the forces between particles, As the number of atom increases, the number of interactions grows rapidly, making direct analytical or numerical solutions impractical. With the explicit forms of the kinetic energies and interaction terms, the many-body Hamiltonian for a system consisting of nuclei and electrons becomes:

$$\hat{H} = -\sum_{I} \frac{\hbar^2}{2M_I} \nabla^2_{\mathbf{R}_I} - \sum_{i} \frac{\hbar^2}{2m_e} \nabla^2_{\mathbf{r}_i} + \frac{1}{2} \sum_{I \neq J} \frac{Z_I Z_J e^2}{|\mathbf{R}_I - \mathbf{R}_J|} + \frac{1}{2} \sum_{i \neq j} \frac{e^2}{|\mathbf{r}_i - \mathbf{r}_j|} - \sum_{I,i} \frac{Z_I e^2}{|\mathbf{R}_I - \mathbf{r}_i|}. \tag{2.4}$$

Here, the indicates I, J run over the nuclei, while i and j run over the electrons, $\mathbf{R}_I$ and $\mathbf{M}_I$ are the position and mass of nuclei, respectively. $\mathbf{r}_i$ and $\mathbf{m}_e$ are the position and mass of electrons. $|\mathbf{R}_I - \mathbf{R}_J|$, $|\mathbf{R}_I - \mathbf{R}_I|$ and $|\mathbf{r}_i - \mathbf{r}_j|$ represent the distant between nuclei-nuclei, nuclei–electrons, and electrons–electrons, respectively. $\mathbf{Z}_I$ is the atomic number of the I–th nucleus. Solving the many-body Hamiltonian is challenging due to the high dimensionality of the wave function, electron-electron correlations, the Pauli exclusion principle, and complex nucleus interactions. Analytical solutions are only possible for simple systems like the Hydrogen atom, as most many–body systems with multiple electrons and nuclei cannot be solved exactly.

2.2.1 Born–Oppenheimer Approximation

The Born–Oppenheimer approximation simplifies the many–body Schrödinger equation by treating the nuclei as fixed in space due to their much greater mass compared to electrons. This allows the electronic wave functions to be solved independently, reducing the complexity of the system. Under this approximation, the total Hamiltonian can be expressed as a sum of two parts: the electronic Hamiltonian $\hat{H}_{el}$, which describes the motion of electrons in the field of fixed nuclei, and the nuclear Hamiltonian $\hat{H}_{nuc}$, which accounts for the motion of the nuclui interacting with each other. The total Hamiltonian $\hat{H}$ is then given by:

$$\hat{H} = \hat{H}_{el} + \hat{H}_{nuc} \tag{2.5}$$

Where

$$\hat{H}_{el} = -\sum_{i} \frac{\hbar^2}{2m_e} \nabla^2_{r_i} + \frac{1}{2} \sum_{i,j} \frac{e^2}{|r_i - r_j|} - \sum_{I,i} \frac{Z_I e^2}{|R_I - r_i|} \tag{2.6}$$

and

$$\hat{H}_{nuc} = \sum_{I} \frac{\hbar^2}{2M_I} \nabla^2_{\mathbf{R}_I} + \frac{1}{2} \sum_{I,J} \frac{Z_I Z_J e^2}{|\mathbf{R}_I - \mathbf{R}_J|}. \tag{2.7}$$

The Born–Oppenheimer approximation simplifies calculations by treating nuclei as fixed, focusing on the electronic structure. If nuclear motion is important, their quantum–mechanical behavior can be included, with the total energy being the sum of electronic and nuclear energies [25]. This dual approach captures the intricate interplay between electronic and nuclear dynamics, providing a comprehensive view of the energy of the system by accounting for both contributions. Once the electronic Hamiltonian $\hat{H}_{el}$ is defined, the electronic Schrodinger equation can be expressed as:

$$\hat{H}\Psi(r_1, r_2, \ldots, r_N) = E\Psi(r_1, r_2, \ldots, r_N). \tag{2.8}$$

The many-body Schrödinger equation is challenging to solve due to the complexity

of the wave function and electron–electron correlations. While approximations allow calculations for simple systems like H_2^+, further approximations are needed for larger systems.

2.2.2 Hartree–Fock Approximation and its Limitations

The Hartree–Fock approximation approximates the many–body wave function using a Slater determinant, which ensures antisymmetry by combining electron orbitals and making the wave function change sign when two electrons are exchanged. Despite it advantage, The Hartree–Fock approximation has limitations, primarily its neglect of electron correlation effects, as it assumes a mean-field approximation. This can lead to inaccuracies in properties like bond lengths, reaction energies, and excitation energies, especially in systems with strong electron correlations. Furthermore, while the Slater determinant effectively accounts for the antisymmetry of the wave function, it does not capture the dynamic correlation between electrons, which arises from their instantaneous interactions. Additionally, the computational cost of the Hartree–Fock method scales as $O(N^4)$, where N is the number of electrons in the system. This scaling arises because the method involves calculating integrals over all pairs of electron orbitals. As the number of electrons increases, the number of required calculations grows rapidly, making it computationally expensive for larger systems.

2.3 Density Functional Theory

Density Functional Theory (DFT) is a powerful quantum mechanical modeling method widely used to investigate the electronic structure of many-body systems. Unlike traditional methods that rely on wave functions, DFT is based on the electron density, which is considered a fundamental variable. The key idea behind DFT is that all properties of a system can be determined from its electron density rather than the many–body wave function. This approach simplifies the problem of solving the Schrödinger equation, as it reduces the complexity associated with many–body interactions. DFT is particularly advantageous because it balances ac-

curacy and computational efficiency, allowing researchers to study larger and more complex systems than would be feasible with wavefunction–based methods. By leveraging the Hohenberg-Kohn theorems and the Kohn-Sham equations, DFT provides a practical framework for exploring a wide range of physical, chemical, and material properties [26, 27].

2.3.1 The Electron Density

In Density Functional Theory (DFT), the electron density $n(r)$ serves as the central variable for describing a quantum system. The electron density represents the probability of finding an electron at a particular point in space and can be derived from the many–body wave function $\Psi(r_1, r_2, \ldots, r_N)$ by integrating over all electron coordinates. This relationship is expressed mathematically as:

$$\hat{H}_{el}\Psi(r_1, r_2, \ldots, r_N) = E\Psi(r_1, r_2, \ldots, r_N). \tag{2.9}$$

Additionally, we must remember that all electrons are identical; thus, we cannot label them as electron 1 or electron N. Instead, we can determine the probability of any order or set of N electrons being located at the coordinates r_1 to r_N. While the wave function contains comprehensive information about the quantum state of a system, it is the electron density that ultimately determines all measurable properties. The total number of electrons N in the system can also be calculated from the electron density using the equation:

$$N = \int n(r)\, dr. \tag{2.10}$$

This integration highlights that the electron density encodes vital information about the total number of electrons, making it a fundamental aspect of DFT. By focusing on $n(r)$ instead of the complex multidimensional wave function, DFT simplifies calculations, making it a practical and efficient approach for studying the electronic structure of various materials.

2.3.2 Hohenberg-Kohn Theorems

Density Functional Theory (DFT) was established in 1964 by Hohenberg and Kohn, whose theorems laid the foundation for linking electron density to quantum system properties, making DFT a key alternative to wave–function–based methods. The Hohenberg–Kohn theorems are central to the formulation of DFT, and they can be summarized as follows:

First theorem: The ground-state electron density $n(r)$ uniquely determines the external potential $V_{ext}(r)$ acting on the electrons. This means that if the electron density of a system is known, the external potential can be uniquely inferred, allowing for the derivation of all ground-state properties, including the total energy, from the electron density.

The first Hohenberg–Kohn theorem states that the ground–state electron density uniquely determines the external potential, and thus the Hamiltonian and wave function. The proof assumes two different potentials yielding the same density, leading to a contradiction, confirming the one–to–one relationship, Ψ and Ψ', with $\hat{H}\Psi = E_0\Psi$ and $\hat{H}'\Psi' = E_0'\Psi'$. Since Ψ' is not the ground state of $\hat{H}$, it follows that

$$E_0 < \langle\Psi'|\hat{H}|\Psi'\rangle < \langle\Psi'|\hat{H}'|\Psi'\rangle + \langle\Psi'|\hat{H} - \hat{H}'|\Psi'\rangle < E_0' + \int n_0(r)[V_{ext}(r) - V_{ext}'(r)]\,dr \tag{2.11}$$

similarly

$$E_0' < \langle\Psi|\hat{H}'|\Psi\rangle < \langle\Psi|\hat{H}|\Psi\rangle + \langle\Psi|\hat{H}' - \hat{H}|\Psi\rangle < E_0 + \int n_0(r)[V_{ext}'(r) - V_{ext}(r)]\,dr. \tag{2.12}$$

Adding this equation (11) and equation (12) leads to the contribution,

$$E_0 + E_0' < E_0 + E_0' \tag{2.13}$$

Hence, no two different external potentials $V_{ext}(r)$ can give rise to the same ground state density $V_{ext}(r)$ which determines the external potential $V_{ext}(r)$, except for a constant. That is to say, there is a one–to–one mapping between the ground state

density $V_{ext}(r)$ and the external potential $V_{ext}(r)$, although the exact formula is unknown.

Second theorem: For any trial electron density $n(r)$), the energy functional $E[n]$ will yield a value that is greater than or equal to the ground-state energy E_0. The equality holds when the trial density corresponds to the true ground-state density. This variational principle implies that one can minimize the energy functional $E[n]$ with respect to the electron density to find the ground state of a system. There exists a universal functional $F[n(r)]$ of the density, independent of the external potential $V_{ext}(r)$, such that the minimum value of the energy functional

$$E[n(r)] \equiv \int n(r)V_{ext}(r)\,dr + F[n(r)] \tag{2.14}$$

yields the exact ground-state energy of the system. The exact ground–state density $n_0(\mathbf{r})$ minimizes this functional. Thus, the exact ground–state energy and density are fully determined by the functional $E[n(r)]$. The universal functional $F[n(r)]$ can be written as:

$$F[n(r)] \equiv T[n(r)] + E_{int}[n(r)] \tag{2.15}$$

where $T[n(r)]$ is the kinetic energy and $E_{int}[n(r)]$ is the interaction energy of the particles. According to the variational principle, for any wave function Ψ', the energy functional

$$E[\Psi'] \equiv \langle \Psi' | \hat{T} + \hat{V}_{int} + \hat{V}_{ext} | \Psi' \rangle \tag{2.16}$$

reaches its global minimum only when Ψ' is the ground–state wave function Ψ_0, with the constraint that the total number of particles is conserved. According to the first Hohenberg–Kohn theorem,Ψ' must correspond to a ground state with particle density $n'(r)$ and external potential $V_{ext}(r)$, making $E[\Psi']$ a functional of $n'(r)$. Applying the variational principle:

$$E[\Psi'] = \int n'(r)V'_{ext}(r)\,dr + F[n'(r)] > E[\Psi_0] = \int n_0(r)V_{ext}(r)\,dr + F[n_0(r)] = E[n_0(r)] \tag{2.17}$$

Thus, the energy functional

$E[\Psi'] = \int n'(r)V'_{ext}(r)\,dr + F[n'(r)] > E[\Psi_0] = \int n_0(r)V_{ext}(r)\,dr + F[n_0(r)] = E[n_0(r)]$ evaluated for the correct ground–state density $n_0(r)$ is lower than the value of this functional for any other density $n(r)$. Therefore, by minimizing the total energy functional of the system with respect to variations in the density $n(r)$, one can find the exact ground–state density and energy. This functional, however, only determines ground-state properties and does not provide any insight into excited states.

2.3.3 Advantage and Disadvantage of Hohenberg–Kohn Theorems

The Hohenberg–Kohn theorems, fundamental to density functional theory (DFT), simplify computational chemistry by relating ground–state properties directly to electron density instead of complex wave functions. The first theorem ensures a unique mapping between electron density and external potential, while the second introduces a variational principle for optimizing density. This shift enables efficient, accurate modeling of systems from small molecules to large biological structures.
Despite their importance, the Hohenberg–Kohn theorems have limitations: they apply only to ground states, offering no direct insight into excited states, and the accuracy of DFT depends heavily on the choice of exchange-correlation functional. DFT may struggle with strong electron correlations, and calculating exchange–correlation energies can still be computationally demanding. Additionally, reliance on external potentials and challenges in interpreting electron density require careful application in complex systems.

2.3.4 Kohn-Sham Equation: Reforming Many-body Problems

The Kohn–Sham equation is a fundamental element of density functional theory (DFT), derived from the Hohenberg-Kohn theorems, which establish the unique relationship between ground–state electron density and external potential. By transforming the complex many–body problem into an equivalent system of non-interacting

single–particle equations, the Kohn–Sham approach enables accurate and computationally efficient electronic structure calculations for a wide range of systems. In the Kohn–Sham approach, the true interacting electron system is mapped onto an auxiliary system of non–interacting electrons that yield the same electron density as the original system. This is achieved through the Kohn-Sham equations, which can be expressed as:

$$-\frac{\hbar^2}{2m_e}\nabla^2\psi_i(\mathbf{r}) + V_{eff}(\mathbf{r})\psi_i(\mathbf{r}) = \epsilon_i\psi_i(\mathbf{r}), \tag{2.18}$$

Where, $V_{eff}(r)$ is the effective potential that includes the external potential and the exchange-correlation potential. The Kohn–Sham orbitals $\psi_i(r)$ are used to construct the electron density $n(r)$ as:

$$n(r) = \sum_i |\psi_i(r)|^2. \tag{2.19}$$

This approach significantly reduces the complexity of solving the many–body Schrödinger equation by allowing for the treatment of a system of independent particles, while still capturing the essential effects of electron correlation through the exchange–correlation functional. The effective potential in the Kohn–Sham framework can be expressed as:

$$V_{eff} = V_{ext} + V_{Hartree}[n(r)] + V_{xc}[n(r)]. \tag{2.20}$$

Here, V_{ext} represents the external potential acting on the electrons in the system. This potential typically arises from the interaction between the electrons and fixed nuclei or any other external fields applied to the system. In many cases, V_{ext} is described by the Coulomb potential due to the nuclei, reflecting how electrons experience attraction towards positively charged atomic cores. This term plays a crucial role in determining the overall potential landscape in which the electrons move, significantly influencing the electronic structure of the system. The term $V_{Hartree}[n(r)]$ is the Hartree potential, which describes the classical electrostatic interaction between electrons in a many–body system. It accounts for the repulsion between charged particles, reflecting that the potential energy experienced by an electron

is due to the distribution of other electrons around it. The Hartree potential is calculated as:

$$V_{Hartree}[n(r)] = e^2 \int \frac{n(r')}{|r - r'|}\, dr'. \tag{2.21}$$

This formulation integrates the electron density $n(r)$ over all space, considering the effect of all other electrons on a given electron located at r. This approach provides a mean–field treatment of electron-electron repulsion, avoiding the complexity of considering every pair of interactions explicitly. The exchange-correlation potential $V_{xc}[n(r)]$ represents the quantum mechanical effects of exchange and correlation among electrons. It is defined as:

$$V_{xc}[n(r)] = \frac{\delta E_{xc}[n]}{\delta n}. \tag{2.22}$$

The exchange term arises from the antisymmetry requirement of the total wave function for fermions, accounting for the reduction in energy when two electrons are spatially separated. The correlation term reflects the correlated motion of electrons that cannot be captured by a mean–field approach, accounting for the ways in which the presence of one electron affects the probability distribution of another electron's position and momentum. From these considerations, the Kohn–Sham Hamiltonian can be formulated as:

$$\hat{H}_{KS} = -\frac{\hbar^2}{2m_e}\nabla^2 + V_{ext} + V_{Hartree}[n(r)] + V_{xc}[n(r)]. \tag{2.23}$$

The Kohn–Sham formulation improves upon the Hartree method by incorporating exchange and correlation effects into the effective potential, enabling a more accurate description of many–body systems. In condensed matter physics, the Kohn–Sham approach iteratively refines the ground-state electron density by solving single-particle equations starting from an initial density, updating the effective potential, and recalculating the density until self-consistency is achieved. The self–consistent Kohn–Sham procedure is performed iteratively, updating the electron density until

convergence is achieved based on criteria like energy change, density variation, or atomic forces. If not converged, densities are mixed and the cycle repeats. Once self-consistency is reached, key physical quantities such as total energy, forces, stress, eigenvalues, density of states, and band structure can be calculated.

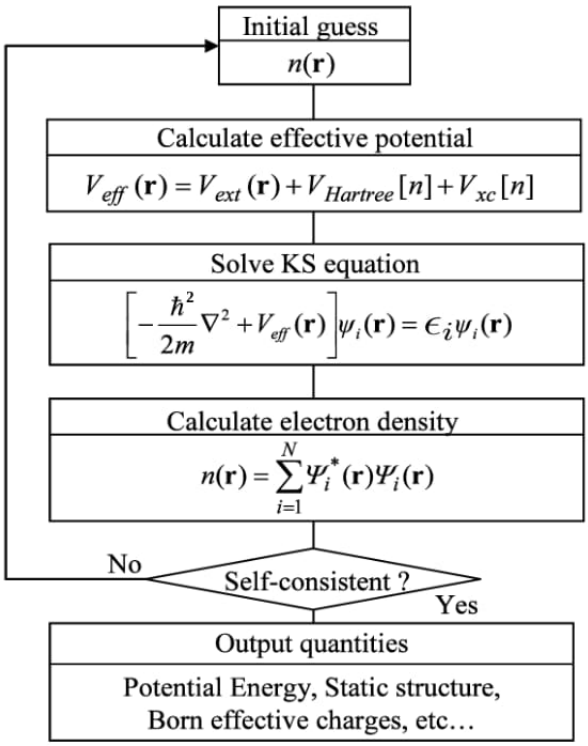

Figure 2.1: Flowchart illustrating the iterative process for solving the Kohn-Sham equation in density functional theory to obtain the ground-state electron density and associated propertie of a many-body system

2.3.5 The Role and calculation of Exchange-Correlation

In density functional theory, the exchange–correlation potential V_{xc} is approximated, often using the Local Density Approximation (LDA), which assumes V_{xc} depends only on the local electron density, similar to a homogeneous electron gas [28]. While simple, LDA can perform reasonably well for certain materials, especially solids with nearly uniform electron densities. The Generalized Gradient Approximation (GGA) improves upon LDA by incorporating electron density gradients, offering better accuracy for varying densities. Hybrid functionals, like $B3LYP$, further enhance accuracy by mixing exact Hartree-Fock exchange with LDA or GGA exchange-

correlations. In practice, the calculation of V_{xc} is an iterative process within the self-consistent field(SCF) method. The DFT algorithm begins with an initial guess for the electron density, usually based on atomic configurations. Using this initial density, the Kohn-Sham equations are solved to update the potential and electron density. The exchange–correlation potential, V_{xc}, is recalculated at each step based on the updated density. This process continues until the electron density converges to a self-consistent solution, meaning that the input and output densities agree within a set tolerance. Recent developments also include meta-GGA functionals, which incorporate even higher–order density-related terms, such as the kinetic energy density, to account for more complex interactions. While computationally more expensive, these functionals can offer improved accuracy for systems with intricate electronic structures. Thus, although V_{xc} is not known exactly, various approximations–from LDA and GGA to hybrid and meta–GGA functionals allow DFT to achieve a good balance between accuracy and computational efficiency for a wide range of materials and molecular systems [29].

Chapter 3

Results and Discussion

In this chapter, first-principles calculations based on Density Functional Theory (DFT) have been employed to investigate the structural, electronic, mechanical, optical, and thermoelectric properties of Ca_2VTlO_6. Computational tools provide an efficient and accurate means of predicting material behavior at the atomic level, which is especially valuable for newly designed or experimentally challenging materials. These simulations allow detailed exploration of intrinsic properties without the limitations of experimental boundary.

3.1 Computational Method

The structural, electronic, optical, mechanical and thermoelectric properities of Ca_2VTlO_6 double perovskites have been investigated using the full–potential linearized augmented plane wave (FP–LAPW) method within the framework of density functional theory (DFT), as implemented in the WIEN2k package [30]. Lattice parameters of Ca_2VTlO_6 were optimized in the simple cubic structure with the space group $Fm\bar{3}m$ using Birch-Murnaghan equation of state. To obtain more accurate band gap calculations for the electronic properties, the local density approximation (LDA) was used in combination with the modified Becke-Johnson (mBJ) poten-

tial developed by Tran and Blaha. We used it to optimize the ground states of Ca_2VTlO_6, with the mBJ potential minimizing the electronic band gap. For the double perovskite Ca_2VTlO_6, the RMT values for Ca, V, Tl, and O are 2.0, 1.7, 2.5, and 1.4 a.u., respectively. After optimizing the energy, we set $R_{\mathrm{MT}} \times K_{\max} = 8$, where R_{MT} represents the smallest radius of the muffin–tin sphere, and $K_{\max}$ is the largest reciprocal lattice vector used in the plane wave function expansion. The number of k-points was chosen as 3500 for SCF (Self Consistent Field) calculations in the Brillouin zone and 17500 for the DOS calculation. The energy and charge convergence limits for the iteration process were set to 0.0001 Ry and 0.0001 e, where e is the charge of electron. $G_{\max}$=16 $\mathrm{Ry}^{\frac{1}{2}}$. Charpin's method describes the elastic behavior of a material with a perfectly cubic structure using three independent elastic constants: C_{11}, C_{12}, and C_{44}. Finally, the thermoelectric properties are determined using the BoltzTraP code, which applies the rigid band approximation and classical transport theory.

3.2 Structural properties

The structure of the double perovskite Ca_2VTlO_6 is generated in this study using the XcrysDen software in combination with the WIEN2k package. The crystal structure of the double perovskite Ca_2VTlO_6 belongs to the space group $Fm\bar{3}m$ and exhibits a cubic arrangement. The unit cell structure of the double perovskites is illustrated in figure 3.1(a), which consists of ten atoms. The lattice constant of the structure is 8.093 Å. The atoms Ca, V, Tl and O occupy the following Wyckoff positions: Ca at (0.25, 0.25, 0.25), V at (0.5, 0.5, 0.5), Tl(0.269, 0, 0) and O at (0.0, 0.0, 0.0). The volume optimization is allowed for the determination of minimum energy which is displayed by the system . Now it is clear that, every system tries to its ground state. So we plotted total energy vs unit cell volume of the compounds which is shown in the figure 3.1(b). By applying the Murnaghan fit, we find that a volume of 132.40 $\mathrm{Å}^3$ corresponds to a calculated minimum energy of -46106.767 Ry. The lattice constant of the primitive unit cell was optimized and used to construct the complete crystal structure, after which the total energy of the conventional unit cell

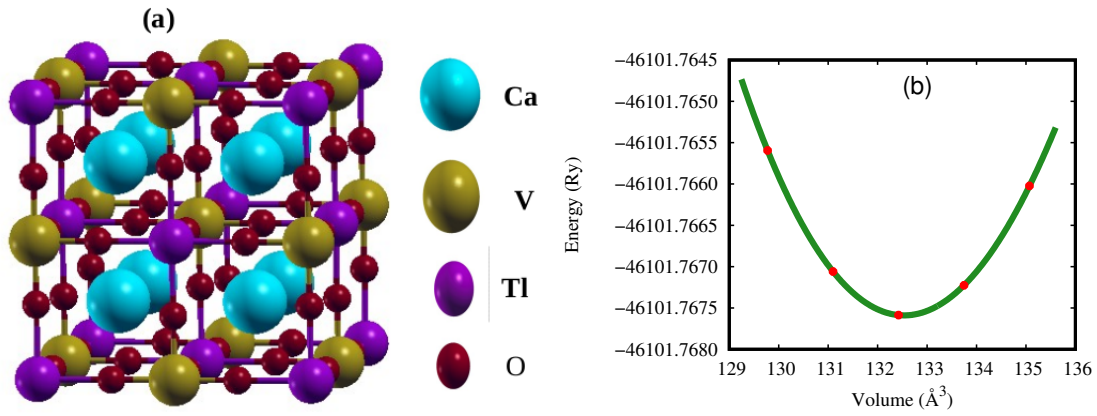

Figure 3.1: The crystal structure and Energy vs Volume of double perovskite Ca_2VTlO_6

was calculated. The Birch-Murnaghan equation of state represent by:

$$E(V) = E_0 + \frac{9V_0B_0}{16}\left\{\left[\left(\left(\frac{V_0}{V}\right)^{\frac{2}{3}} - 1\right)^3 B_0'\right] + \left[\left(\left(\frac{V_0}{V}\right)^{\frac{2}{3}} - 1\right)^2 \left(6 - 4\left(\frac{V_0}{V}\right)^{\frac{2}{3}}\right)\right]\right\}. \tag{3.1}$$

In this equation, V_0 and V are the ground state unit cell volume and deformed unit cell volume, E_0 is the energy of the ground state, B_0 is the bulk modulus and B_0 is its derivative.

3.3 Electronic properties

The calculation of the electronic properties, including band structure and density of states, offer valuable insights into the optical properties of the materials under investigation. To determine the DOS and band structure, we use the mBJ potential, which contributes a more accurate band gap compared to the PBE approximation and experimental data. The partial density of states is crucial for understanding the contributions of different angular momentum components. The electron density helps in understanding the chemical bonding in Ca_2VTlO_6, supporting the formation of its ionic bond and covalent bond. In this section, we discussed the electronic band structure, density of states, and electron density, respectively.

3.3.1 Band structure

Understanding the electronic band structure is essential for comprehending the physical properties of crystalline solids, which largely determine their optical and transport properties. A key objective of this work is to calculate the band structure and assess the band gap of the double perovskite Ca_2VTlO_6 . The evaluated band struc-

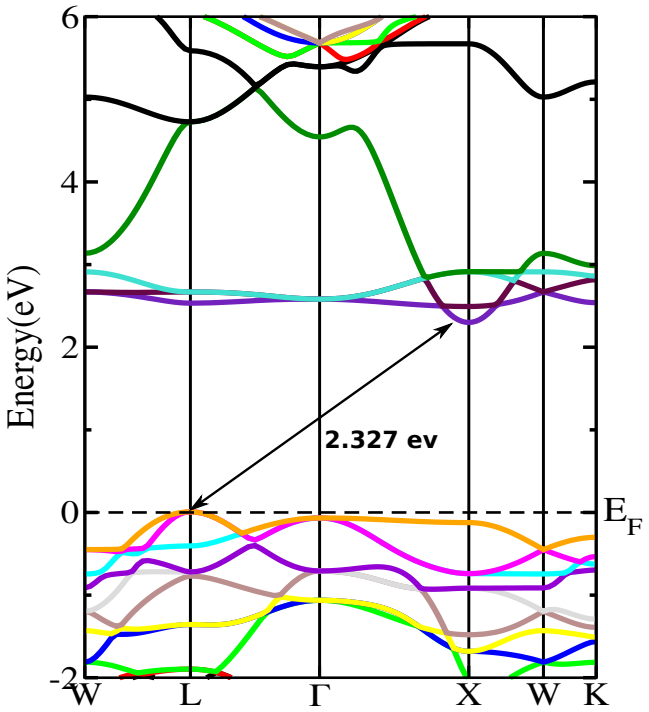

Figure 3.2: The band structure Ca_2VTlO_6

ture of Ca_2VTlO_6 is shown in Figure 3.2. The figure shows that there is no overlap between the conduction band and the valence band at the Fermi level. The black horizontal dashed line at 0 eV indicates the Fermi level, set to zero. The valence band (VB) and conduction band (CB) are represented as colored lines located below and above the Fermi energy, respectively. In the first Brillouin zone, the conduction band minimum is located along the X symmetry direction, while the valence band maximum is located along the L symmetry direction. From the band structure, it is clear that the double perovskite Ca_2VTlO_6 exhibits an indirect band gap semiconductor behavior, as the valence band maximum and conduction band minimum

are located at different points in the first Brillouin zone.

3.3.2 Density of state

The Density of States (DOS) describes the number of available quantum states at each energy level that electrons can occupy in a material. It provides a distribution of energy levels and how densely packed those levels are at different energies. The Partial Density of States (PDOS) decomposes the Total Density of State (TDOS) into contributions from specific atoms, orbitals, or subgroups of the material. This allows us to see which atoms or orbitals are contributing to the electronic states at different energy levels. The calculated TDOS and PDOS without spin polarization are shown in Figure 3.3 and Figure 3.4, respectively. A comprehensive study of

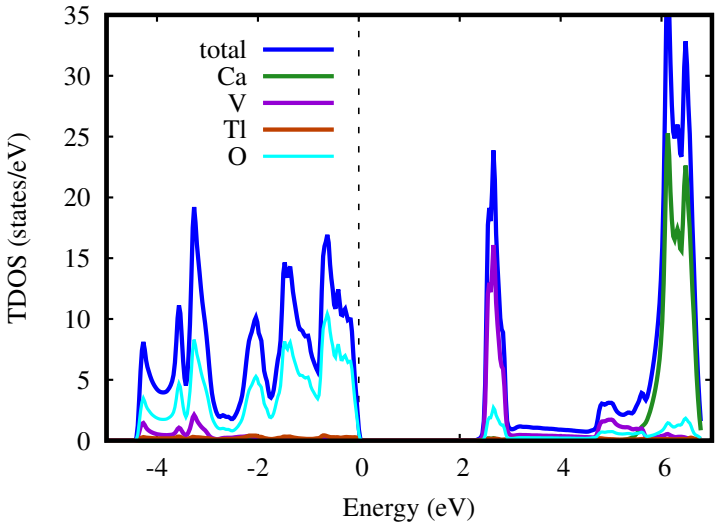

Figure 3.3: Total density of states for double perovskite Ca_2VTlO_6

energy band formation requires calculating the density of states (DOS) of the system. The calculated Fermi energy for the atoms is 0.489 eV. From previous section, we got the band gap approximately 2.327 eV for mBJ potential which indicates that the compound is semiconductor. In the total DOS, oxygen (O) mainly contributes to the valence band (VB), whereas thallium (Tl) primarily dominates the conduction band (CB), exceeding the contributions of other atoms. We accepted the contributions of s, p, d, f orbitals for the Tl and V atoms, s, p, d orbitals for the Ca atom, and s, p orbitals for the O atom. From Figure 3.4(a), we can observe that the contribution

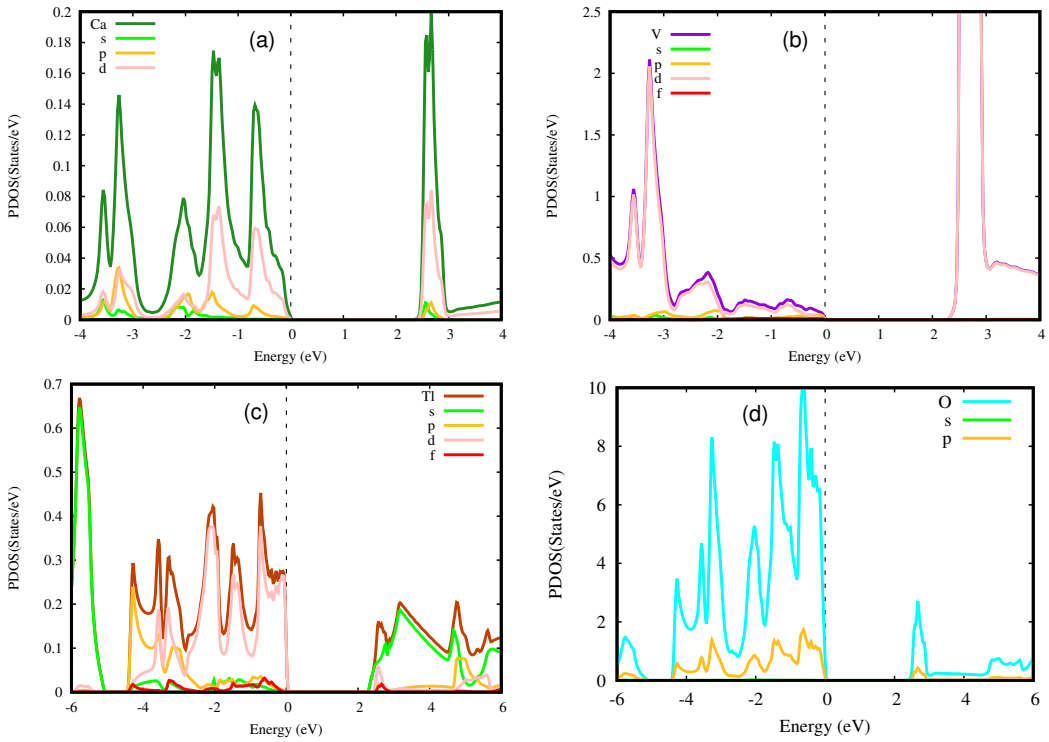

Figure 3.4: The calculated partial density of states of Ca, Tl, V, O atoms for Ca_2VTlO_6 double perovskite

of electrons from the Ca atom in the conduction band is greater than in the valence band, where the d orbitals contribute, but the s and p orbitals do not contribute significantly. The figure 3.4(b) shows that for the V atom, the d orbital in the conduction band (CB) dominates over the other orbitals. From Figure 3.4(c), we observe that the majority of the peaks are in the valence band region, though a significant peak is also present in the conduction band region. There is a larger electron contribution from the s and d orbitals than from the s and p orbitals. At present, looking at Figure 3.4(d), we can observe that the electrons of O atoms are mostly located in the valence band region rather than the conduction band region, and the p orbital electrons have a higher concentration than the s orbital electrons.

3.3.3 Electron density

The electron density distributions along the (100) and (110) planes of Ca_2VTlO_6 reveal strongly localized electron clouds around Tl and O atoms, with minimal interatomic overlap. This localization and the absence of density bridges suggest that Tl–O bonding is predominantly ionic, characterized by electron transfer from

Tl to O. Minor polarization effects may introduce slight covalency, but the bonding remains overwhelmingly ionic across both planes.

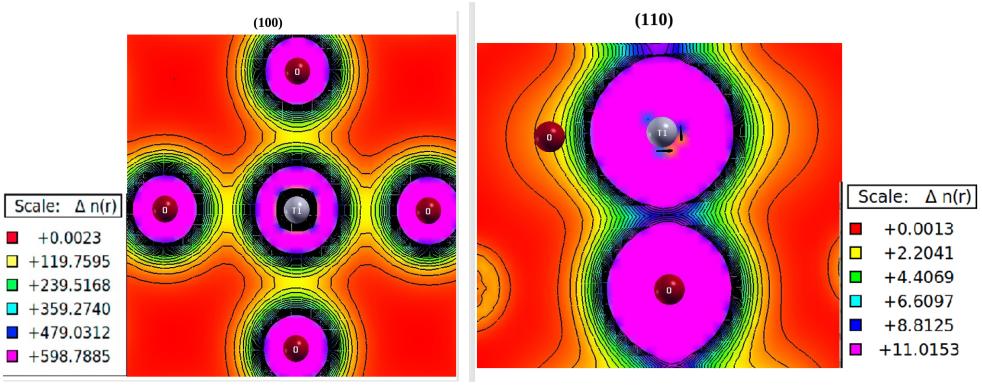

Figure 3.5: The calculated electron density for (100) and (110) plane

3.4 Optical properties

To evaluate a material's performance in optoelectronic device applications, it is essential to understand its optical properties. Optical properties describes how material interacts with light. We have calculated all the parameters using The TB–mBJ potential. To investigate the optical properties of Ca_2VTlO_6 double perovskite material, we calculated its dielectric function, absorption coefficient, optical conductivity, reflectivity and refractive index.

3.4.1 Dielectric function

The complex dielectric function of a material represents the relationship between its energy band structure and optical transition . The complex dielectric function of the semiconductor material is given by:

$$\varepsilon(\omega) = \varepsilon_1(\omega) + i\varepsilon_2(\omega) \tag{3.2}$$

Where, $\varepsilon_1(\omega)$ and $\varepsilon_2(\omega)$ are the real and imaginary dielectric function. The dielectric function helps explain how an electromagnetic field impacts a materials optical response. The real and imaginary dielectric functions for Ca_2VTlO_6 were derived from

the mBJ potential, as shown in the Figure 3.6, where energy is polotted in the X axis and the real and imaginary dielectric functions plotted on the Y axis. The real

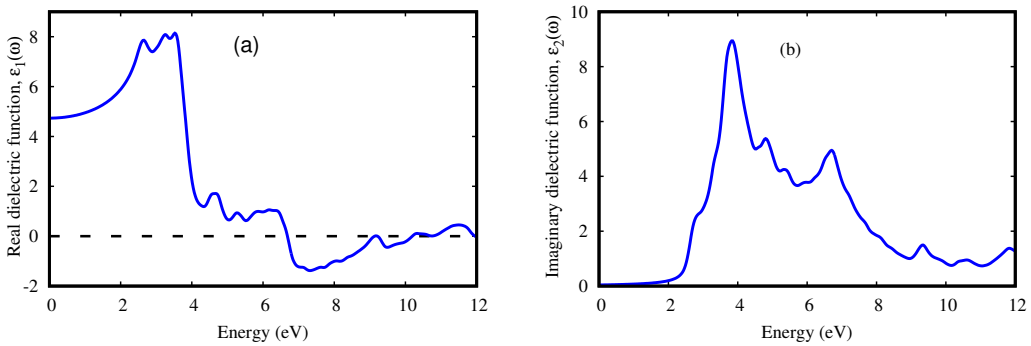

Figure 3.6: Real and Imaginary part of dielectric function for Ca_2VTlO_6 double perovskite

part of the dielectric function, $\varepsilon_1(\omega)$ is a measure of how a material responds to an external electric field in terms of polrization. From the figure 3.6(a), we can analyze the behaviour of $\varepsilon_1(\omega)$ as a function of energy , offering optical and electronic property. The high dielectric constant at low energies suggests strong polarization, while the peak and subsequent decline reflect electronic transitions and energy absorption. The negative values at higher energies indicate reflective metallic-like behavior. The imaginary dielectric function plays a crucial role in describing how these materials interact with light shown in the figure 3.6(b). It provides insights into absorption mechanisms driven by electronic transitions and is essential for understanding their behavior in optoelectronic applications. By examining $\varepsilon_2(\omega)$, we can predict and optimize the performance of double perovskites in devices such as solar cells, LEDs, and other photonic technologies.

3.4.2 Optical conductivity

Optical conductivity is a material property that describes the relationship between the induced current density in the material and the magnitude of the applied electric field at various frequencies. This is directly related to the electronic structure of the material. the nature of the bonding and the band structure affects how electrons respond to an electric field. If the material is metallic or semi-metallic, the optical

conductivity will be higher as electrons are more easily excited to higher energy states by the applied field . The optical conductivity exhibits a pronounced feature near 4 eV, indicating strong electronic transitions. its energy is illustrated in Figure 3.7. The range of energy extends from 0 to approximately 14 eV. Higher photon energy corresponds to transitions involving higher-energy electronic states in the material. The Figure of Y axis represents the optical conductivity and The values range from 0 to 5000. The optical conductivity is close to zero, indicating that there is likely an optical band gap in this material. The optical conductivity can be represented by the following equation,

$$\sigma(\omega) = \sigma_1(\omega) + i\sigma_2(\omega) \tag{3.3}$$

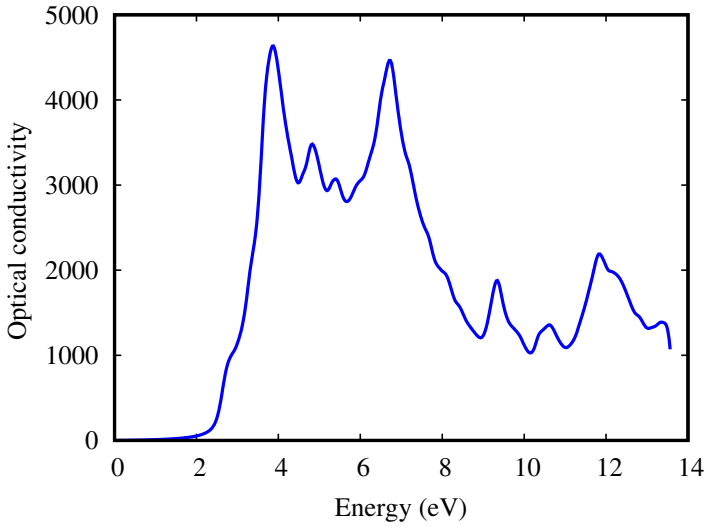

Figure 3.7: Optical conductivity

This means the material does not absorb or conduct light below this threshold, as photons with energy less than the band gap cannot excite electrons. A sharp increase in optical conductivity occurs around 2 eV, suggesting the onset of electronic transitions due to photon absorption. This likely corresponds to the material's band gap energy, marking the start of interband transitions. The graph shows a large peak in optical conductivity near 4 eV, which suggests strong electronic transitions. This peak could be due to energy band transitions, where electrons move between different energy bands, indicating a high density of electronic states in this region

and making the material potentially useful in light-harvesting devices, such as solar cells or photodetectors. The oscillatory behavior in higher energy ranges indicates that the material can interact with a broad spectrum of light, including ultraviolet (UV) radiation.

3.4.3 Absorption coefficient

The absorption coefficient is a fundamental physical parameter that quantifies how effectively a material absorbs electromagnetic radiation and attenuates its intensity. The absorption coefficient evaluates a material's suitability for shielding applications or functioning as an anti-reflective coating. The absorption coefficient can be followed by the equation:

$$\alpha(\omega) = \frac{\sqrt{2}\,\omega}{c}\left[\sqrt{\varepsilon_1^2(\omega) + \varepsilon_2^2(\omega)} - \varepsilon_1(\omega)\right]^{1/2} \tag{3.4}$$

The following figure shows the absorption coefficient as a function of energy, calculated using the mBJ potential. Figure 3.8 shows the absorption coefficient of Ca_2VTlO_6. From the Figure, we can observe that the absorptivity gradually in-

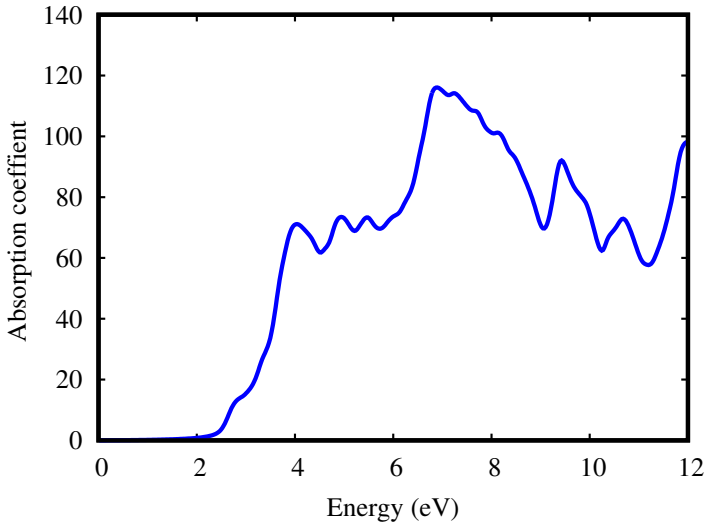

Figure 3.8: Absorption coefficient

creases in the infrared and visible regions, peaks at 7 eV in the ultraviolet region, and then decreases as the energy continues to increase. The absorption peak reveals

that this material can absorb photons in both the ultraviolet and visible ranges. This makes it an excellent candidate for use in electro-optical applications within the visible region.

3.4.4 Reflectivity

Optical reflectivity is an important parameter that influences the transition of electrons from the valence band to the conduction band. It is a key optical property that describes the proportion of light reflected from a surface relative to the amount of incident light. Reflectivity depends on several factors, including the material's electronic structure, surface roughness, and angle of incidence [31]. The expression for the reflectivity $R(\omega)$ is given by,

$$R(\omega) = \left| \frac{\sqrt{\varepsilon(\omega)} - 1}{\sqrt{\varepsilon(\omega)} + 1} \right|^2 \tag{3.5}$$

Figure 3.9 illustrates the variation of optical reflectivity with different energies for our material. The Figure shows that the Ca_2VTlO_6 double perovskite reflects incident light at energies below its band gap. After crossing the band-gap energy, it suddenly exhibits a prominent peak at 4.33 eV before continuing forward. This also

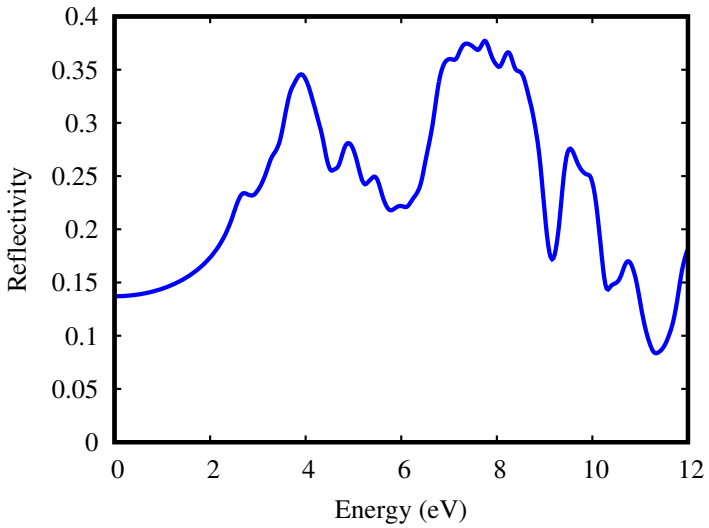

Figure 3.9: Optical reflectivity

indicates that the maximum reflectivity of the material occurs at 8 eV, where it

reaches approximately 35%. This suggests that at this energy, the material is most reflective, and the percentage of light reflected is about 35%. The total reflectivity over the entire energy range will be lower than this peak due to the decreasing reflectivity at both lower and higher energies. However, the material's overall reflectivity will likely be in the 15%-35% range, depending on the exact integration of reflectivity across all energies.

3.4.5 Refractive index

The refractive index is a fundamental property of materials that describes how light propagates through a medium. It is a dimensionless number that determines the speed and direction of light within the material relative to its behavior in a vacuum. The refractive index and the band gap are inversely related, meaning that as the refractive index increases, the corresponding band gap decreases. The refractive index $n(\omega)$ can be expressed as the square root of the real part of the complex dielectric function,

$$\tilde{n}(\omega) = \sqrt{\frac{\varepsilon_1(\omega) + i\varepsilon_2(\omega)}{2}} \tag{3.6}$$

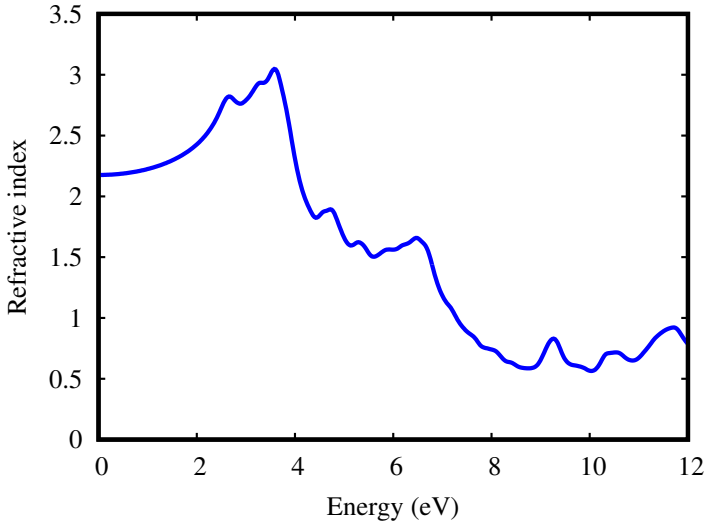

Figure 3.10: Refractive index

The curve of refractive index versus energy is shown in Figure 3.10. From the Figure

we can see that, the refractive index starts at low values, around 0.5, and gradually increases. This behavior indicates that at lower photon energies, the material has a weaker interaction with light. The refractive index is low because the material might be transparent or minimally absorbing at these energies. After reaching a peak near 3 eV. This region corresponds to the onset of significant optical transitions within the material, where the material absorbs and interacts more strongly with light. The refractive index reaches its maximum here, indicating stronger electronic transitions and possible absorption features in the material.

3.5 Mechanical properties

The elastic properties of materials are essential for understanding their strength and behavior [32]. The elastic constants help us better comprehend the mechanical stability of solids. The mechanical properties of materials with cubic symmetry are fully described by the calculated parameters, namely C_{11}, C_{12}, C_{44}. The mechanical stability of a crystal can be evaluated using the Born stability criteria, which for a cubic system are expressed as: $C_{11} - C_{12} > 0$, $C_{11} > 0$, $C_{44} > 0$, $C_{11} + 2C_{12} > 0$ [33]. The existence of the crystal not possible in the stable unless its elastic constants obey the generalized mechanical stability criteria. The elastic constants provide insights into various mechanical properties, such as the Young's modulus (Y), which represents the material's strength; the bulk modulus (B), which indicates the material's stiffness, with higher B values corresponding to greater resistance to compression; and the shear modulus, which describes the material's ability to undergo plastic deformation. The obtained value of the shear modulus is 102.440 GPa, which is small, meaning that the compound shows less plastic twist. To determine the ductile or brittle behavior of $B3LYP$, The bulk and shear moduli, which are key indicators of a material's hardness, can be determined using the Voigt-Reuss-Hill (VRH) averaging schem. The Voigt limits of the bulk modulus (B) and shear modulus (G) for a cubic system are given by the following expressions [34,35]:

$$B_V = \frac{C_{11} + 2C_{12}}{3} \tag{3.7}$$

and,

$$G_v = \frac{C_{11} - C_{12} + 3C_{44}}{5}. \tag{3.8}$$

However, the Reuss formulae for the bulk and shear moduli are:

$$B_v = B_R \tag{3.9}$$

$$G_R = \frac{5(C_{11} - C_{12})C_{44}}{4C_{44} + 3(C_{11} - C_{12})}. \tag{3.10}$$

Young's modulus, which determines the strength of a material, is the ratio of linear stress to strain and can be evaluated using the following relation:

$$Y = \frac{9BG}{3B + G}. \tag{3.11}$$

we calculated Pugh ratio (B/G) ratio, which was found to be 1.4129, indicating a brittle nature.The Cauchy pressure value (C_{11}–C_{44}) can also be used to estimate ductility and brittleness; a material is said to be ductile if its value is positive, and brittle if it is negative. The data in Table 3.1 clearly show that the Cauchy pressure for Ca_2VTlO_6 is negative, highlighting its brittle nature.

C_{11}	C_{12}	C_{44}	C_{12} - C_{44}	B	G	Y	A	B/G	ν
239.74	97.24	130.63	-33.39	144.74	102.44	248.65	1.83	1.41	0.213

Table 3.1: The computed values of elastic constant C_{11}, C_{12}, C_{44}, Cauchy's pressure of C,Bulk modulus (B), Shear modulus (G), Young's modulus(Y), elastic anisotrophy factor (A), Pugh ratio (B/G) and poisson's ratio (ν) of Ca_2VTlO_6

Poisson's ratio is another criterion used to determine the ductility and brittleness of a compound. The material has a ductile character if its value is more than 0.26; if not, it is regarded as brittle. Table also shows that Poisson's ratio for Ca_2VTlO_6 is close to 0.213, which confirms its brittle nature. So from the calculated data, we can say that, Elastic constants are frequently used to evaluate the mechanical firms its brittle nature. characteristics and structural stability of a material. It is crucial to uncover information about the binding properties between neighboring atomic planes, along with the anisotropic nature and structural stability.

3.6 Thermoelectric properties

The thermoelectric properties of Ca_2VTlO_6 were predicted using the BoltzTraP computational code [36]. To reduce environmental pollution and prevent energy crises, thermoelectric materials have gained significant interest for their ability to convert waste heat into useful electricity [37–39]. Thermoelectric parameters such as Seebeck coefficient(S), Figure of merit(ZT), power factor($S^2\sigma$), electronic conductivity(σ) and thermal conductivity are against temperature in figure 3.11. he efficiency of a thermoelectric material is typically evaluated using the dimensionless figure of merit, ZT, which is defined as:

$$ZT = \frac{S^2\sigma T}{\kappa} \tag{3.12}$$

which behavior calculating by BoltzTrap program [40] . Figure (a) illustrates the vibration of electrical conductivity with temperature (T) in the range of 200 to 1000 K for double perovskite. The calculated results indicate a linear increase in electronic conductivity with increasing temperature. As a result the material exhibits semiconductor-like behavior. As temperature rises, more energy is available to excite electron from the valence band to conduction band. This leads to an increase in the number of free charge carrier, enhancing conductivity and may overcome scattering effects caused by structural defects, allowing for better mobility of charge carriers. In Figure (b), the electronic part of the thermal conductivity $\left(\frac{\kappa_e}{\tau}\right)$ also increases with temperature, showing a nonlinear yet consistent upward moving. The graph clearly shows that thermal conductivity rises with temperature. An increase in thermal conductivity means the material becomes more efficient at conductivity heat and unusual behavior where phonon scattering decreases with temperature might allow phonon to carry more heat. Figure (c) presents the variation of the power factor ($S^2\sigma$) with temperature. The power factor combines both the electronic conductivity and the square of the Seebeck coefficient and serves as a direct indicator of a material's ability to convert thermal energy into electrical energy. The power factor increases steadily with temperature, suggesting that the material is increasingly

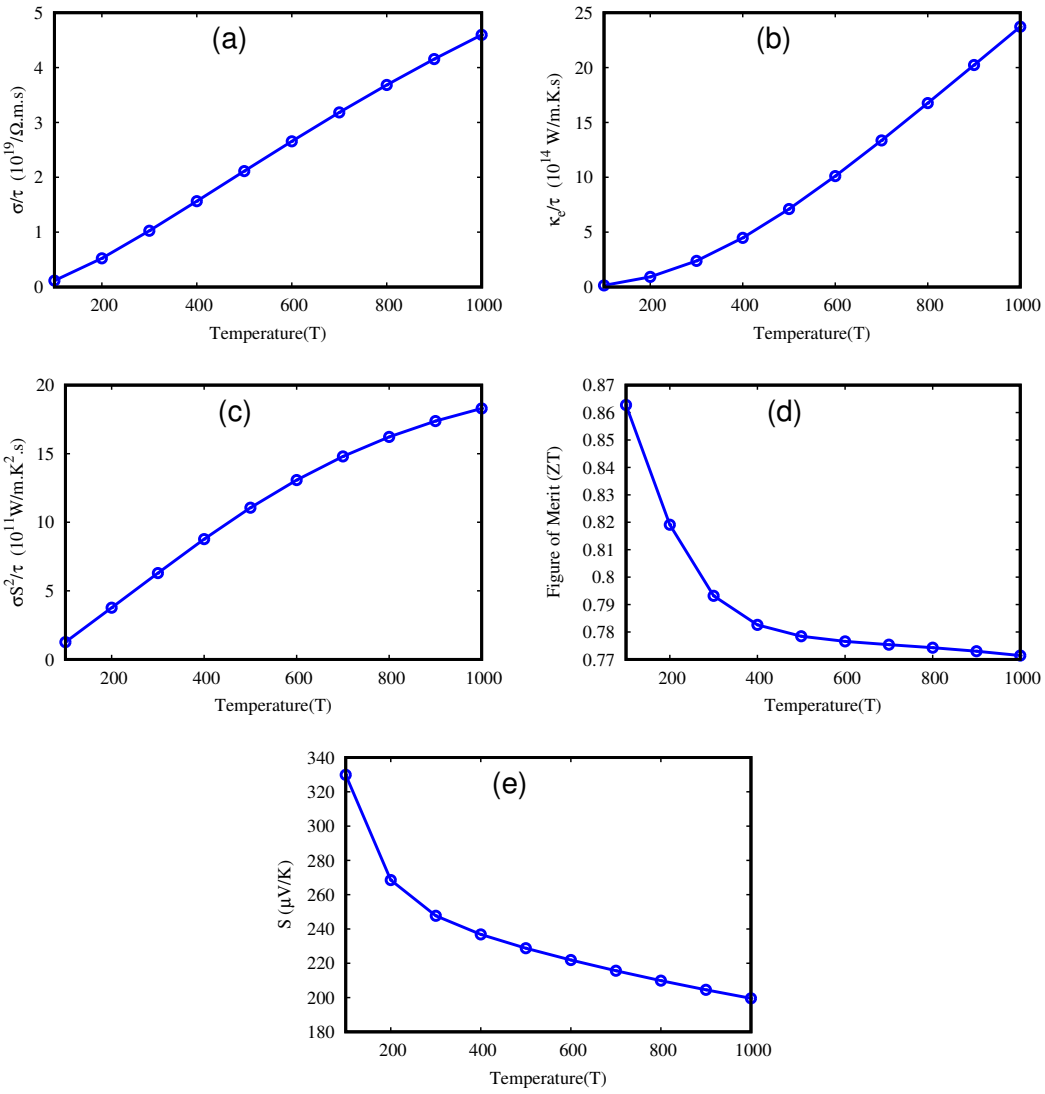

Figure 3.11: Thermoelectric properties as (a) Electrical conductivity, (b) Thermal conductivity , (c) Power factor, (d) Figure of merit, (e) Seebeck coefficient

efficient in thermoelectric energy conversion at higher temperatures—assuming constant or optimized doping levels. The dimensionless Figure of merit (ZT), shown in Figure (d), provides a comprehensive evaluation of the material's thermoelectric efficiency. It depends on the Seebeck coefficient, electronic conductivity, and total thermal conductivity. Interestingly, Figure of merit exhibits a maximum value of approximately 0.86 at 200 K, after which it gradually decreases with rising temperature. This behavior indicates that although the electronic performance improves with temperature, the total thermal conductivity—especially its lattice contribution—may increase more rapidly, reducing the overall ZT. The decrease in Figure of merit suggests that this material is more suitable for low-temperature thermoelectric

applications, where thermal losses are minimized. At room temperature, the estimated values of the Figure of merit is 0.79. And this value indicate that Ca_2VTlO_6 is a promising candidate for thermoelectric device application. Figure (e) displays the Seebeck coefficient (S) as a function of temperature. The Seebeck coefficient initially shows a high value of about 320 μV/K at 200 K, which is desirable for thermoelectric materials. However, as temperature increases, the Seebeck coefficient steadily decreases, which is commonly observed in semiconductors. This decreasing value can be attributed to the increase in intrinsic carrier concentration and possible onset of bipolar conduction, where both electrons and holes contribute to transport, reducing the net Seebeck effect. the examined material demonstrates favorable thermoelectric properties at lower temperatures, particularly around 200 K, with a high Seebeck coefficient, strong power factor, and peak Figure of merit value. These findings suggest that the material holds strong potential for low-temperature thermoelectric device applications, although optimization of thermal conductivity-especially the lattice component could further enhance its high-temperature performance.

Chapter 4

Summery

In this work, structural, electronic, optical, mechanical, and thermoelectric properties of cubic Ca2VTlO6 double perovskite was performed using the WIEN2k code based on the DFT–based FP–LAPW approach. The lattice parameter is found to be 8.093 Å. The calculated electronic properties indicate that Ca_2VTlO_6 is a semiconductor with an indirect band gap of 2.327 eV, where the lowest energy bands in the conduction region and the highest energy bands in the valence region are located at different symmetry points in the first Brillouin zone. The density of states also confirms that the compound is a semiconductor. It has been confirmed that the electrons in oxygen atoms mainly contribute to the valence band, while Ca dominates the conduction band in comparison to the other atoms. The charge density provides insights into the ionic interactions, particularly between Ca and O. The optical characteristics show variations, with the maximum refractive index Occupying from the visible to the ultraviolet, highlighting their potential for solar cells and other optoelectronic applications. The responsive optical properties of Ca_2VTlO_6, especially its wide refractive index range, make it highly suitable for optoelectronic applications such as photodetectors and LEDs, highlighting its potential for practical device implementation. An analysis of the mechanical properties indicates that the material is brittle, with Poisson's ratio and Pugh's ratio being less than 0.26

and 1.75, respectively. The computed thermoelectric properties, obtained using the BoltzTraP code, reveal that as the temperature increases, electrical conductivity, thermal conductivity, and power factor increase, while the Seebeck coefficient and Figure of merit decrease. The results highlight the potential of Ca2VTlO6 for application in optoelectronic devices.

Bibliography

[1] Huanping Zhou, Qi Chen, Gang Li, Song Luo, Tze Bing Song, Hsin Sheng Duan, Ziruo Hong, Jingbi You, Yongsheng Liu, and Yang Yang. Interface engineering of highly efficient perovskite solar cells. *Science*, 345(6196):542–546, 2014.

[2] Julian Burschka, Norman Pellet, Soo-Jin Moon, Robin Humphry-Baker, Peng Gao, Peng Gao, Mohammad K Nazeeruddin, and Michael Grätzel. Sequential deposition as a route to high-performance perovskite-sensitized solar cells. *Nature*, 499(7458):316—319, July 2013.

[3] Andrew Barnabas Wong, Minliang Lai, Samuel Wilson Eaton, Yi Yu, Elbert Lin, Letian Dou, Anthony Fu, and Peidong Yang. Growth and Anion Exchange Conversion of $CH_3NH_3PbX_3$ Nanorod Arrays for Light-Emitting Diodes. *Nano Letters*, 15(8):5519–5524, August 2015.

[4] Erjin Zheng, B. Yuh, G. A. Tosado, and Qiuming Yu. Solution-processed visible-blind uv-a photodetector based on chnhpbcl perovskite thin films. *Journal of Materials Chemistry C*, 5(15):3796–3806, 2017.

[5] Christopher Eames, Jarvist M. Frost, Piers R. F. Barnes, Brian C. O'Regan, Aron Walsh, and M. Saiful Islam. Ionic transport in hybrid lead iodide perovskite solar cells. *Nature Communications*, 6(1):7497, 2015.

[6] Tianhao Wu, Xiao Liu, Xinhui Luo, Xuesong Lin, Danyu Cui, Yanbo Wang, Hiroshi Segawa, Yiqiang Zhang, and Liyuan Han. Lead-free tin perovskite solar cells. *Joule*, 5(4):863–886, 2021.

[7] Joseph S. Manser, Jeffrey A. Christians, and Prashant V. Kamat. Intriguing optoelectronic properties of metal halide perovskites. *Chemical Reviews*, 116(21):12956–13008, 2016.

[8] H. Wang, W. Su, J. Liu, and C. Wang. Recent development of n-type perovskite thermoelectrics. *Journal of Materiomics*, 2(3):225–236, 2016.

[9] Sanjay Pachori, Rohit Agarwal, Akash Shukla, Upasana Rani, and Ajay Singh Verma. Mechanically stable with highly absorptive formamidinium lead halide perovskites ($HC(NH_2)_2PbX_3$; X = Br, Cl): Recent advances and perspectives. *International Journal of Quantum Chemistry*, 121(15):e26671, 2021.

[10] Guichuan Xing, Nripan Mathews, Shuangyong Sun, Swee Sien Lim, Yeng Ming Lam, Michael Grätzel, Subodh Mhaisalkar, and Tze Chien Sum. Long-range balanced electron- and hole-transport lengths in organic-inorganic chnhpbi. *Science*, 342(6156):344–347, 2013.

[11] Kyle Frohna, Tejas Deshpande, John Harter, Wei Peng, Bradford A. Barker, Jeffrey B. Neaton, Steven G. Louie, Osman M. Bakr, David Hsieh, and Marco Bernardi. Inversion symmetry and bulk rashba effect in methylammonium lead iodide perovskite single crystals. *Nature Communications*, 9(1):1829, 2018.

[12] Giacomo Giorgi, Jun-Ichi Fujisawa, Hiroshi Segawa, and Koichi Yamashita. Small photocarrier effective masses featuring ambipolar transport in methylammonium lead iodide perovskite: A density functional analysis. *The Journal of Physical Chemistry Letters*, 4(24):4213–4216, 2013.

[13] Xiaojun Qin, Zhiguo Zhao, Yidan Wang, Junbo Wu, Qi Jiang, and Jingbi You. Recent progress in stability of perovskite solar cells. *Journal of Semiconductors*, 38(1):011002, 2017.

[14] Pradeep R. Varadwaj. Aagcrcl (a = li, na, k, rb, cs) halide double perovskites: a transition metal-based semiconducting material series with appreciable optical characteristics. *Physical Chemistry Chemical Physics*, 22(42):24337–24350, 2020.

[15] N.A. Noor, M. Waqas Iqbal, Taharh Zelai, Asif Mahmood, H.M. Shaikh, Shahid M. Ramay, and Waheed Al-Masry. Analysis of direct band gap ascini (a = rb, cs) double perovskite halides using dft approach for renewable energy devices. *Journal of Materials Research and Technology*, 13:2491–2500, 2021.

[16] Hongwei Lei, David Hardy, and Feng Gao. Lead-free double perovskite csagbibr: Fundamentals, applications, and perspectives, 2021.

[17] A.A. AlObaid, S.A. Rouf, T.I. Al-Muhimeed, A.I. Aljameel, S. Bouzgarrou, H.H. Hegazy, T. Alshahrani, G. Nazir, A. Mera, and Q. Mahmood. New lead-free double perovskites (rbgecl/br): A promising material for renewable energy applications. *Materials Chemistry and Physics*, 271:124876, 2021.

[18] Yongjun Tian, Bo Xu, and Zhisheng Zhao. Microscopic theory of hardness and design of novel superhard crystals. *International Journal of Refractory Metals and Hard Materials*, 33:93–106, 2012.

[19] Sami Vasala and Maarit Karppinen. Abbo perovskites: A review. *Progress in Solid State Chemistry*, 43(1-2):1–36, 2015.

[20] Kang Yi, Qingkai Tang, Zhiwei Wu, and Xinhua Zhu. Unraveling the structural, dielectric, magnetic, and optical characteristics of nanostructured La_2NiMnO_6 double perovskites. *Nanomaterials*, 12(6):979, 2022.

[21] D. D. Sarma, E. V. Sampathkumaran, Sugata Ray, R. Nagarajan, Subham Majumdar, Ashwani Kumar, G. Nalini, and T. N. Guru Row. Magnetoresistance in ordered and disordered double perovskite oxide sr_2femoo_6. *Solid State Communications*, 114(9):465–468, 2000.

[22] David J. Griffiths. *Introduction to Quantum Mechanics*. Pearson Prentice Hall, 2nd edition, 2005.

[23] Robert G. Parr and Weitao Yang. Density-functional theory of the electronic structure of molecules. *Annual Review of Physical Chemistry*, 46(1):701–728, 1995.

[24] Klaus Capelle. A bird's-eye view of density-functional theory. *Brazilian Journal of Physics*, 36(4A):1318–1343, 2006.

[25] Michael P. Marder. *Condensed Matter Physics*. John Wiley & Sons, Hoboken, NJ, 2nd edition, 2010.

[26] David C. Young. Density functional theory. In *Computational Chemistry: A Practical Guide for Applying Techniques to Real-World Problems*, pages 42–48. John Wiley & Sons, 2001.

[27] Wolfram Koch and Max C. Holthausen. *A Chemist's Guide to Density Functional Theory*. John Wiley & Sons, 2nd edition, 2015.

[28] Pierre Hohenberg and Walter Kohn. Inhomogeneous electron gas. *Physical Review*, 136(3B):B864–B871, 1964.

[29] Walter Kohn and Lu Jeu Sham. Self-consistent equations including exchange and correlation effects. *Physical Review*, 140(4A):A1133–A1138, 1965.

[30] M. Jamal, S. Jalali Asadabadi, Iftikhar Ahmad, and H. A. Rahnamaye Aliabad. Elastic constants of cubic crystals. *Computational Materials Science*, 95:592–599, 2014.

[31] Jakiul Islam and A. K. M. Akther Hossain. Narrowing band gap and enhanced visible-light absorption of metal-doped non-toxic cssncl3 metal halides for potential optoelectronic applications. *RSC Advances*, 10(13):7817–7827, 2020.

[32] Subhash Chandra Lakkad. Temperature dependence of the elastic constants. *Journal of Applied Physics*, 42(10):4277–4281, 1971.

[33] Yuanyuan Kong, Yonghua Duan, Lishi Ma, and Runyue Li. Phase stability, elastic anisotropy and electronic structure of cubic MaL_2 (M = Mg, Ca, Sr and Ba) laves phases from first-principles calculations. *Materials Research Express*, 3(10):106505, 2016.

[34] J. A. D. Matthew. Dynamical theory of crystal lattices by m. born and k. huang. *Acta Crystallographica Section A*, 26(6):702, 1970.

[35] Woldemar Voigt. *Lehrbuch der Kristallphysik*. Teubner, Leipzig, 1928.

[36] Georg K. H. Madsen and David J. Singh. Boltztrap. a code for calculating band-structure dependent quantities. *Computer Physics Communications*, 175(1):67–71, 2006.

[37] Yingzhi Zhou, Jing Wang, Dongxiang Luo, Dehua Hu, Yonggang Min, and Qifan Xue. Recent progress of halide perovskites for thermoelectric application. *Nano Energy*, 94:106949, 2022.

[38] Sile Hu, Zhilin Ren, Aleksandra B. Djurisic, and Andrey L. Rogach. Metal halide perovskites as emerging thermoelectric materials. *ACS Energy Letters*, 6:3882–3905, 2021.

[39] Andreas Kaltzoglou and Polycarpos Falaras. Recent developments on hybrid perovskite materials for solar energy conversion and environmental protection. *Current Opinion in Chemical Engineering*, 33:100708, 2021.

[40] E. Yu. Peresh, V. I. Sidei, and O. V. Zubaka. Phase relations in the systems A_2TeI_6–Tl_2TeI_6 (A = K, Rb, Cs) and A_2TeBr_6–A_2TeI_6 (A = K, Rb, Cs, Tl(I)). *Inorganic Materials*, 41:298–302, 2005.